Limits of hydrosphere-lithosphere interaction: Origin of the lowest-known $\delta^{18}O$ silicate rock on Earth in the Paleoproterozoic Karelian rift

I.N. Bindeman[1]*, A.K. Schmitt[2], and D.A.D. Evans[3]
[1]Department of Geological Sciences, 1272 University of Oregon, Eugene, Oregon 97403, USA
[2]Department of Earth and Space Sciences, University of California–Los Angeles, Los Angeles, California 90095, USA
[3]Department of Geology and Geophysics, Yale University, 210 Whitney Avenue, New Haven, Connecticut 06520-8109, USA

ABSTRACT

Geologic records of Earth's hydrosphere and meteoric precipitation older than 2 Ga are rare, although they provide insight into the past climate, rates of water-rock interaction, and intensity of plate tectonics. Here we report and describe in detail the lowest known $\delta^{18}O$ (–16‰ to –25‰) terrestrial silicate rocks on Earth, found in Paleoproterozoic plagiogneisses from the Belomorian complex, Karelia, Russia. Geochronologic and oxygen isotopic data on zircons (+7‰ to –26‰) and monazite (–17.5‰) imply that the protoliths of these rocks were ca. 2.5 Ga metasediments and metavolcanics that were hydrothermally altered prior to 1.85 Ga within an intracontinental rift zone, and involved ultralow $\delta^{18}O$, <–25‰ meteoric water. Paleogeographic reconstructions indicate that Karelia was at low to middle latitudes throughout the Paleoproterozoic Era. Ultradepleted $\delta^{18}O$ waters outside of polar regions or the interiors of large landmasses provide independent evidence for a moderately glaciated, so called "slushball" Earth climate between 2.45 and 2.4 Ga, in which low- or mid-latitude, mid-size continents were covered with glaciers while the ocean remained at least partially unfrozen to allow for intracontinental isotopic distillation in a large temperature gradient. In addition to these climatic inferences, the data are more readily explained by a depleted –10‰ seawater reservoir during Paleoproterozoic time.

INTRODUCTION

In the modern world, oxygen and hydrogen isotope ratios of <0‰ (Vienna standard mean ocean water) exist only in water that went through the Rayleigh evaporation-precipitation cycle, the most negative values being characteristic of polar regions and continental interiors (e.g., Criss and Taylor, 1986). Interaction of silicate rocks with meteoric water proceeds in hydrothermal systems when temperature exceeds a certain threshold (~100–300 °C) to initiate kinetics of exchange; at these temperatures the isotopic fractionation between rocks and meteoric water is small (0‰–3‰), and thus at high water/rock ratios, rocks may approach, and record, $\delta^{18}O$ and δD values of water.

Reports of anomalously low $\delta^{18}O$ values (Krylov, 2008; Visotskii et al., 2008), in polymetamorphic plagiogneisses from Karelia, Russia, triggered our investigation. Here we present a detailed microanalytical investigation of the Chupa plagiogneisses of the Belomorian belt in Karelia (Fig. 1), and report the lowest (–15‰ to –28‰) $\delta^{18}O$ mineral and rock values ever measured in silicate rocks on Earth.

The Belomorian polymetamorphic complex between Kola and Karelia (Fig. 1) is one of many 1.9–1.8 Ga, Paleoproterozoic mobile belts around the world that collectively indicate accretion of the Nuna supercontinent (Zhao et al., 2002). The Belomorian rift closed via collisional kyanite-grade metamorphism ca. 1.85 Ga, followed by rapid exhumation and subsequent residence near the Earth's surface after 1.75 Ga (Bibikova et al., 2004; Terekhov, 2007). The studied corundum (ruby)-kyanite assemblage of Khitostrov and similar deposits along the Belomorian belt (Fig. 1) record a high-Al Archean metagraywacke protolith (Balagansky et al., 1986; Terekhov, 2007), metamorphosed at ~0.7 MPa (~20 km depth). The large size of minerals in leucosome (pegmatitic or diaphtoresis) bodies (Fig. DR4 in the GSA Data Repository[1]) suggests metasomatic recrystallization with abundant participation of fluid during late Paleoproterozoic exhumation.

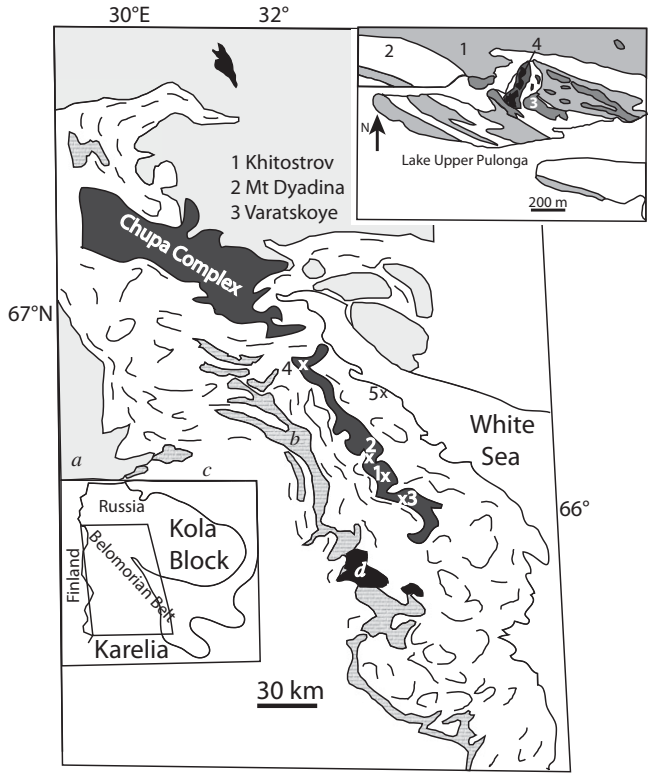

Figure 1. Simplified geologic map of Belomorian belt with structural elements (Balagansky et al., 1986; Bibikova et al., 2004), showing locations of Paleoproterozoic Chupa allochthonous nappe with Khitostrov corundum plagiogneisses (1x), low $\delta^{18}O$ plagiogneiss of Mount Dyadina (2x), and Varatskoye (x3), and two additional localities with similar detrital zircon age distribution (4x, 5x). Map units: *a*—Paleoproterozoic Lapland allochthon; *b*—Archean metavolcanic and metasedimentary rocks; *c*—Other nappes of Belomorian belt; *d*—Gabbro and layered intrusions (2.45–2.4 Ga). Inset, upper right: Distribution of high-Al gneisses in studied locality of Khitostrov (after Serebryakov et al., 2007). 1—kyanite-garnet-biotite plagiogneisses; 2—garnet-biotite plagiogneisses; 3—metamorphosed gabbroids; 4—ruby-bearing corundum gneisses, with large metasomatic pegmatoidal segregations, sampled in this study.

*E-mail: bindeman@uoregon.edu.

[1]GSA Data Repository item 2010170, methods, tables, and supplementary figures, is available online at www.geosociety.org/pubs/ft2010.htm, or on request from editing@geosociety.org or Documents Secretary, GSA, P.O. Box 9140, Boulder, CO 80301, USA.

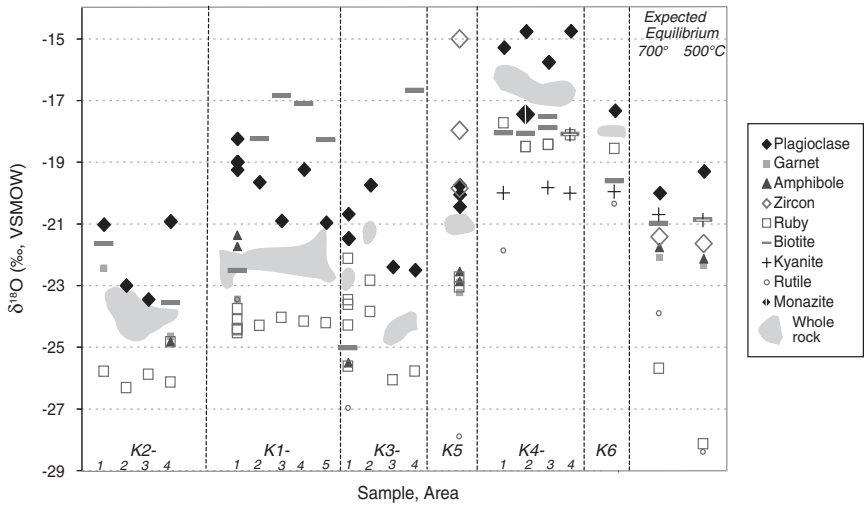

Figure 2. $\delta^{18}O$ values of coexisting single crystals in mineral clusters represented by each vertical array of data points (analyses in Table DR1; see footnote 1). VSMOW—Vienna standard mean ocean water. Each vertical array of data points represents local metamorphic equilibrium that preserves bulk-rock $\delta^{18}O$ value, shown by gray fields. Isotopic equilibrium between minerals is shown on right at 500 °C and 700 °C, inferred temperatures from cation geothermometry (Terekhov, 2007; Krylov, 2008). Note that biotite is higher than equilibrium in samples K1 and K3, which can be explained by 1%–10% retrogressive exchange with higher $\delta^{18}O$, higher δD magmatic or secondary meteoric fluids (see Fig. DR1). Note significant isotopic heterogeneity among different samples (outcrop scale), and among different mineral clusters in same sample (centimeter scale), explained here to reflect protolith variations.

LOWEST $\delta^{18}O$ AND δD VALUES AND THE ORIGINS OF $\delta^{18}O$ HETEROGENEITY

The large size of the studied minerals made them ideal targets for high-precision and high-spatial resolution, single-crystal, within-cluster study by laser fluorination, and D/H analysis (Bindeman, 2008; see the Data Repository for methods). Six samples of corundum- and kyanite-bearing plagiogneisses were investigated in detail for the oxygen isotopic composition of minerals and hydrogen isotopic composition of biotites and amphibole (Fig. 2). Given the complex metamorphic history of these rocks, a particular emphasis was paid to the minor and accessory minerals, i.e., rubies, kyanites, monazites, zircons, and garnet. Due to their extremely slow solid-state oxygen diffusion (and thus high closure temperatures), these refractory minerals record $\delta^{18}O$ values of the protolith from the time of peak metamorphic initial growth (e.g., Valley, 2001). Such minerals, except zircon, appear to be in overall high-temperature isotopic equilibrium with the rock-forming mineral plagioclase (Fig. 2).

Individual biotites and bulk amphibole crystals from mineral clusters demonstrate highly depleted δD values, as low as –167‰, with variation parallel to the meteoric water line. Other amphiboles (–130‰ to –166‰) and more altered biotite (–83‰ to –189‰; Table DR1 and Fig. DR1 in the Data Repository) are still remarkably low; only the alteration mineral chlorite records higher δD values (–55‰). Isotopic mass-balance calculations require only 1%–20% of high-temperature exchange of an initial –220‰ Paleoproterozoic hydrogen with a variety of younger higher δD metamorphic or secondary waters. These processes have increased $\delta^{18}O$ and δD values of some biotites, but had limited impact on other minerals, and on the major element oxygen. We conclude that the remarkably low $\delta^{18}O$ (and low δD) values characterize the values of the protolith.

Based on single-crystal investigation, we discovered 9‰ $\delta^{18}O$ heterogeneity between studied samples of similar mineralogy and chemistry (Fig. 2) spaced 10–80 m from each other, and as much as 3‰ heterogeneity of rubies within a single 10 cm hand specimen. Furthermore, single large rubies and kyanites exhibit ~1.5‰ isotopic zoning. Given that the amount of retrogressive exchange is limited for these refractory minerals, all these features can be attributed to the initial source heterogeneity prior to mineral growth.

New isotopic values for the Khitostrov corundum deposits (Fig. 2) are the lowest $\delta^{18}O$ values ever measured in silicate materials on Earth. The $\delta^{18}O$ values that we obtained are more negative than values recently reported for Khitostrov and the other two outcrops of corundum "metasomatites" (Mount Dyadina and Varatskoye; Fig. 1; see Krylov and Glebovitsky, 2007). Taken together, these measurements provide a picture of a widespread >50 km linear depletion zone of rocks of similar mineralogy and age within the Belomorian belt. We discount proposed interpretations of low $\delta^{18}O$ values as synmetamorphic or metasomatic, and question their alleged origin as weathering crusts (Krylov, 2008). We infer that high-temperature water-rock exchange can explain the low and heterogeneous $\delta^{18}O$ values. The Karelian $\delta^{18}O$ values are also significantly lower, by more than 10‰–15‰, than those reported for two other localities with strongly depleted $\delta^{18}O$; i.e., Dabie Shan-Sulu in China (Rumble and Yui, 1998; Zheng et al., 2004) and Kokchetav, Kazakhstan (Masago et al., 2003).

U-Th-Pb AGES AND $\delta^{18}O$ VALUES OF ZIRCONS AND MONAZITE

The electron microprobe U-Th-Pb dating of seven monazite grains in sample K4 (Table DR2) yielded a mean age of 1.89 ± 0.009 Ga (1σ, n = 45) and showed no age zoning or grain-to-grain age heterogeneity. The dated monazites have very low $\delta^{18}O$ values of –17.5‰ that are consistent with overall equilibrium with other minerals (Fig. 2) and published regional metamorphic ages from the Belomorian complex (Fig. 3). Zircons from sample K5 yielded $\delta^{18}O$ values of –20‰ (bulk population), –18‰ (large crystals only), and –15‰ (air-abraded grains); by mass balance we may estimate normal $\delta^{18}O$ (~+4‰ – +8‰) cores, and ~–22‰ to –25‰ rims, values in equilibrium with the host mineral assemblage.

Ion microprobe dating coupled with in situ $\delta^{18}O$ measurements in 15 zircons in sample K5 (Fig. 3; Appendix and Table DR2) identified a bimodal population with concordant ages of 2.75–2.45 Ga, +4‰ – +8‰ $\delta^{18}O$ zircons, and 1.9–1.8 Ga, –23‰ to –27‰ zircons and rims; a few analyses of intermediate age and $\delta^{18}O$ are suspected to be due to domain mixing within the spot size of the 20–30 μm ion microprobe beam. The detrital zircon cores (~1000–1500 ppm U and 5–170 ppm Th), and especially younger metamorphic and/or metasomatic rims (~500 ppm U, and <10 ppm Th), have very high U/Th ratios and featureless, dull cathodoluminescence.

Due to very sluggish oxygen isotope diffusion in zircon (Watson and Cherniak, 1997; Valley, 2001), it is the only mineral in the assemblage in which cores survived the Belomorian metamorphism to record protolith age and $\delta^{18}O$ values. Because monazite closes to O-isotope exchange at lower temperatures than zircon (e.g., ~500 °C; Cherniak et al., 2004), the lack of detrital monazite grains and low $\delta^{18}O$ values and ages reflect diffusive exchange and recrystallization during the 1.89 Ga exhumation.

DISCUSSION: ANCIENT METEORIC-HYDROTHERMAL SYSTEM IN A PALEOPROTEROZOIC RIFT

We interpret that heterogeneous and ultralow $\delta^{18}O$ and δD values in minerals from the Belomorian belt record a heterogeneous low $\delta^{18}O$

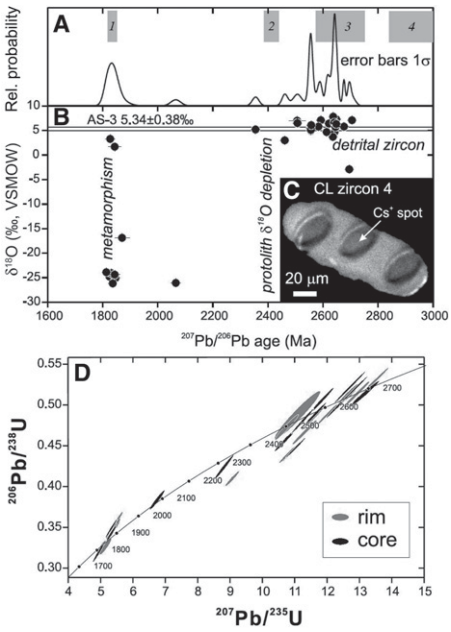

Figure 3. Zircon ages and $\delta^{18}O$ values determined by ion microprobe in sample K5 demonstrating peaks of normal $\delta^{18}O$ (+7‰ – +8‰), concordant zircon ages at 2.7–2.45 Ga representing detrital cores, and low $\delta^{18}O$ (–23‰ to –26‰), ca. 1.85 Ga zircons and rims related to Belomorian metamorphism. A: Age histogram; gray bands denote published ion microprobe zircon ages from other rocks across Belomorian belt (Bibikova et al., 2004; Serebryakov et al., 2007) showing similar age patterns: 1—rims of zircons in similar pegmatites, 2—zircons from regional gabbro, 3—predominant detrital zircons and zircons from metamorphic migmatites and granites, 4—oldest detrital cores. B: $\delta^{18}O$ vs. age diagram; $\delta^{18}O$ analyses were performed on previously dated spots after repolishing. We attribute intermediate ages and $\delta^{18}O$ values due to repolishing and core-rim beam overlap. C: Inset shows dull cathodoluminescence image of zircon 14. D: U-Pb concordia diagram.

protolith that exchanged at high temperatures with ultralow $\delta^{18}O$ meteoric waters prior to metamorphism, and acquired heterogeneity through variable water/rock ratios common to meteoric-hydrothermal systems (Criss and Taylor, 1986). Modern-day shallow meteoric-hydrothermal systems, such as those in calderas of Yellowstone and rift zones of Iceland, are capable of large-scale modification of hundreds of cubic kilometers of crust, and generate highly heterogeneous $\delta^{18}O$ values at centimeter scale (Fournier, 1989). However, because exchange between rocks and water rarely proceeds to completion and requires pervasive water-rock ratios >>1 (Criss and Taylor, 1986), the lowest measured $\delta^{18}O$ value of minerals that we report may correspond to the highest $\delta^{18}O$ value of the altering meteoric water. We estimate that the water that caused Belomorian depletion could have been as low as –30‰ to –35‰, as some of the amphiboles seem to require based on trends in $\delta^{18}O$ and D/H (Fig. DR1). Given the elongated distribution of anomalously low $\delta^{18}O$ corundum-bearing rocks in the Belomorian belt (Fig. 1), an intracontinental rift system would fit the profile well. This inferred intracontinental rift provided favorable magma-driven hydrothermal circulation conditions for removal of ^{18}O and D from rocks by low $\delta^{18}O$, low δD meteoric waters.

POLAR POSITION, SUPERCONTINENT GLACIATION, OR LOW $\delta^{18}O$ SEAWATER?

The occurrence of <–25‰ meteoric water is limited on modern Earth to the Greenland (–25‰ to –45‰) and Antarctic ice sheets (–25‰ to –60‰) (http://www.waterisotopes.org). If one accepts arguments of constancy of $\delta^{18}O$ value of seawater at 0‰ ± 2‰ buffered by nearly constant plate tectonic recycling and/or hydrothermal alteration rates (Muehlenbachs, 1998), then the only way to explain ultradepleted $\delta^{18}O$ values is for the Belomorian rift to be deep within the interior of a large landmass close to the pole, or under an ice cap at polar latitude.

However, paleomagnetic data from Kola and Karelia (Evans and Pisarevsky, 2008) indicate low to moderate paleolatitudes for the Belomorian region at 2.45, 2.06, and 1.88 Ga (Fig. 4), and the most parsimonious interpolation from these data precludes an excursion of the Belomorian region to polar latitudes at any time during the Paleoproterozoic (Fig. 4). Additional constraints can be applied indirectly if one assumes that Kola and Karelia were joined with the Superior craton between initial consolidation ca. 2.7 Ga and separation ca. 2.05 Ga. This reconstruction satisfies both the distribution of precisely dated mafic dike swarms and paleomagnetic data (Mertanen et al., 2006), the latter specifically if it is assumed that the paleomagnetic result shown for 2.45 Ga in Figure 4 is primary. The Superior craton has a much richer data set of demonstrably primary paleomagnetic poles in the 2.45–1.88 Ga interval (references in Fig. 4); this likewise restricts paleolatitudes of its once-juxtaposed cratons to low-moderate latitude throughout that time. Although the original extent of continental continuation between Kola and Karelia and other cratons is unknown (Bleeker, 2003), the rift architecture of sedimentary basins at 2.45 Ga suggests that the Belomorian belt was not deep within the interior of a large supercontinent, thus disallowing the possibility of prolonged intracontinental vapor distillation.

If –30‰ to –35‰ intracontinental waters were to be explained by temperate climate conditions and local alpine glaciation, then an initially depleted seawater of <–10‰ would be required, as more than 15‰–20‰ depletion would be difficult to achieve solely by Rayleigh distillation in the interior of a small to medium-size continent. The initially depleted seawater and Rayleigh distillation would collectively produce <–25‰ alpine snow. Our isotopic and geochronologic data are more consistent with formation of the

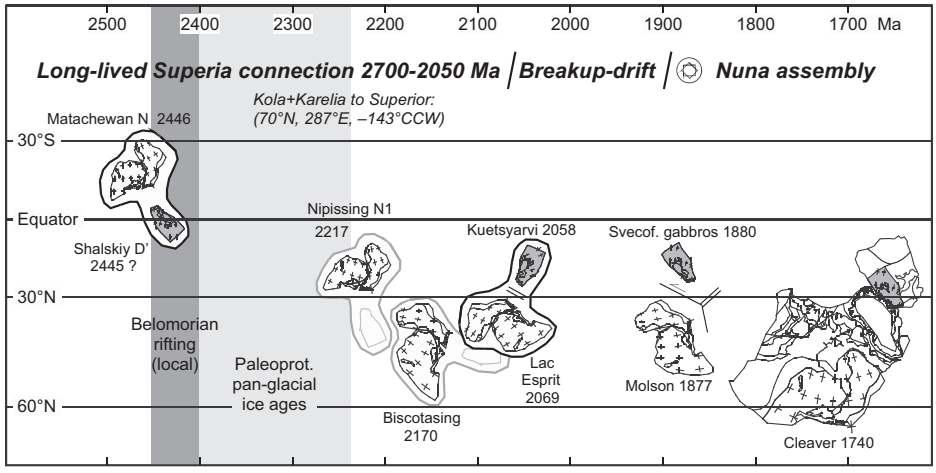

Figure 4. Paleogeographic setting of Belomorian belt. Superior craton (gridded, unshaded) and Kola and Karelia (gridded, shaded) are reconstructed through time, to paleolatitudes (Mercator projection) and orientations according to named paleomagnetic poles (ages in Ma) (Mertanen et al., 2006; Pesonen et al., 2003). Double-line segments schematically indicate rifting; arrow indicates relative transform motion. Long-lived supercraton Superia connection, which likely included other cratons not shown (e.g., Bleeker and Ernst, 2006), is presumed valid throughout interval 2.70–2.05 Ga, permitting paleolatitude assignments for Kola and Karelia inferred by data from Superior craton. Gem symbol indicates metamorphic age of Belomorian gneisses. Reconstruction at 1740 Ma shows Kola and Karelia joined to newly consolidated Laurentia craton (Evans and Pisarevsky, 2008) as part of Nuna supercontinent. Most parsimonious interpolation of Kola and Karelia paleolatitudes precludes any polar excursion between Belomorian rifting (ca. 2.45 Ga) and metamorphism (ca. 1.89 Ga). Svecof.—Svecofennian.

protolith of Chupa gneiss in a ca. 2.45 Ga cold climate period extending to low latitudes in a so called "slushball" regime (Hoffman, 2009). If glaciers reached shores at low latitudes, significant $\delta^{18}O$ and δD gradients inland could have existed by analogy with Greenland (–15‰ to –35‰), aided by the glacial flow supplying lowest $\delta^{18}O$, high-altitude ice to the seashore. Seawater would need to have remained unfrozen to allow for effective evaporation-precipitation cycles inland, thus favoring a "slushball" versus the "hard" snowball model ca. 2.45 Ga. Then, the basalt-generating Belomorian rift zone could have been active in low-latitude, low-altitude, subglacial conditions ca. 2.45 Ga to fit the regional geochronology, amid the recognized global cold climate period (Fig. 4). The 2.45–2.35 Ga stratigraphic record for Kola and Karelia includes abundant mafic rocks and immature sediments of the Sumian and Sariolian successions, indicating rifting accompanied by glaciation (Ojakangas et al., 2001). The presence of a 2.20–2.05 Ga carbonate-evaporite platform with enriched $\delta^{13}C$ and $\delta^{18}O$ values (Melezhik et al., 1999) disallows attainment of the ultralow $\delta^{18}O$ Belomorian values during that interval.

Seawater values of ~–10‰ have been proposed specifically for ca. 2.0 Ga (Burdett et al., 1990), consistent with an overall trend toward decreasing values with increasing age (Jaffres et al., 2007). Such depleted oxygen isotopes in Precambrian carbonate rocks have been interpreted as representing a secular change in either ocean chemistry or temperature (Knauth and Kennedy, 2009; Jaffres et al., 2007). Absolute temperature of the Paleoproterozoic ocean is irrelevant to our conclusions, as long as zonal temperature and precipitation/evaporation gradients remain constant regardless of the global mean. Nonetheless, agreement of the carbonate isotope depletion between Precambrian and Ordovician, the latter time hosting modern-like marine animal ecosystems, favors the model of secular chemical change (Jaffres et al., 2007). We propose that the ultralow, yet heterogeneous, $\delta^{18}O$ values from the Belomorian basic metasediments are best explained by three combined effects: regionally cold glacial climate conditions at low to moderate paleolatitudes, hydrothermal alteration within an early Paleoproterozoic subglacial intracontinental rift, and an initially $\delta^{18}O$-depleted Paleoproterozoic seawater value. While questions remain as to whether a "slushball" Earth is a stable climate state (e.g., Bendsen, 2002), the observations presented here may provide empirical support for it.

ACKNOWLEDGMENTS

We thank two anonymous reviewers for careful reviews, and Paul Hoffman in particular for suggestions leading us to favor a "slush-ball" rather than "snowball" interpretation of our data. This work was supported by National Science Foundation (NSF) grant EAR-CAREER-0844772 and NSF I&F 0732691.

REFERENCES CITED

Balagansky, V.V., Bogdanova, M.N., and Kozlova, N.E., 1986, Evolution of Northwest Belomorian Belt: Apatity, USSR Academy of Sciences, Kola Science Center (in Russian), 100 p.

Bendsen, J., 2002, Climate sensitivity to changes in solar insolation in a simple coupled climate model: Climate Dynamics, v. 18, p. 595–609, doi: 10.1007/s00382-001-0198-4.

Bibikova, E.V., Bogdanova, S.V., Glebovitsky, V.A., Claesson, S., and Skiold, T., 2004, Evolution of the Belomorian Belt: NORDSIM U-Pb zircon dating of the Chupa paragneisses, magmatism, and metamorphic stages: Petrology, v. 12, p. 195–210.

Bindeman, I.N., 2008, Oxygen isotopes in mantle and crustal magmas as revealed by single crystal analysis: Reviews in Mineralogy and Geochemistry, v. 69, p. 445–478, doi: 10.2138/rmg.2008.69.12.

Bleeker, W., 2003, The late Archean record: A puzzle in ca. 35 pieces: Lithos, v. 71, p. 99–134, doi: 10.1016/j.lithos.2003.07.003.

Bleeker, W., and Ernst, R., 2006, Short-lived mantle generated magmatic events and their dyke swarms: The key unlocking Earth's palaeogeographic record back to 2.6 Ga, *in* Hanski, E., ed., Dyke swarms—Time markers of crustal evolution: London, Taylor & Francis, p. 3–26.

Burdett, J.W., Grotzinger, J.P., and Arthur, M.A., 1990, Did major changes in the stable isotope composition of Proterozoic seawater occur?: Geology, v. 18, p. 227–230, doi: 10.1130/0091-7613(1990)018<0227:DMCITS>2.3.CO;2.

Cherniak, D.J., Zhang, X.Y., Nakamura, M., and Watson, E.B., 2004, Oxygen diffusion in monazite: Earth and Planetary Science Letters, v. 226, p. 161–174, doi: 10.1016/j.epsl.2004.07.027.

Criss, R.E., and Taylor, H.P., 1986, Meteoric-hydrothermal systems: Reviews in Mineralogy, v. 16, p. 373–424.

Evans, D.A.D., and Pisarevsky, S.A., 2008, Plate tectonics on the early Earth? Weighing the paleomagnetic evidence, *in* Condie, K., and Pease, V., eds., When did plate tectonics begin?: Geological Society of America Special Paper 440, p. 249–263, doi: 10.1130/2008.2440(12).

Fournier, R.O., 1989, Geochemistry and dynamics of the Yellowstone National Park hydrothermal system: Annual Review of Earth and Planetary Sciences, v. 17, p. 13–51, doi: 10.1146/annurev.ea.17.050189.000305.

Hoffman, P.F., 2009, Pan-glacial—A third state in the climate system: Geology Today, v. 25, p. 100–107, doi: 10.1111/j.1365-2451.2009.00716.x.

Jaffres, J.B.D., Shields, G.A., and Wallmann, K., 2007, The oxygen isotope evolution of seawater: A critical review of a long-standing controversy and an improved geological water cycle model for the past 3.4 billon years: Earth-Science Reviews, v. 83, p. 83–122, doi: 10.1016/j.earscirev.2007.04.002.

Knauth, L.P., and Kennedy, M.J., 2009, The late Precambrian greening of the Earth: Nature, v. 460, p. 728–732.

Krylov, D.P., 2008, Anomalous ratios of $^{18}O/^{16}O$ in corundum-bearing rocks from Northern Karelia: Doklady Earth Sciences, v. 419, p. 533–536, doi: 10.1134/S1028334X08030239.

Krylov, D.P., and Glebovitsky, V.A., 2007, Oxygen isotopic composition and nature of fluid during formation of high-Al corundum-bearing rocks of Mt. Dyadina, Northern Karelia: Doklady Earth Sciences, v. 413, p. 210–212, doi: 10.1134/S1028334X0702016X.

Masago, H., Rumble, D., Ernst, W.G., Parkinson, C.D., and Maruyama, S., 2003, Low $\delta^{18}O$ eclogites from the Kokchetav massif, northern Kazakhstan: Journal of Metamorphic Geology, v. 21, p. 579–587, doi: 10.1046/j.1525-1314.2003.00465.x.

Melezhik, V.A., Fallick, A.E., Medvedev, P.V., and Makarikhin, V.V., 1999, Extreme ^{13}C carb enrichment in ca. 2.0 Ga magnesite-stromatolite dolomite-'red beds' association in a global context: A case for the world-wide signal enhanced by a local environment: Earth-Science Reviews, v. 48, p. 71–120, doi: 10.1016/S0012-8252(99)00044-6.

Mertanen, S., Vuollo, J.I., Huhma, H., Arestova, N.A., and Kovalenko, A., 2006, Early Paleoproterozoic–Archean dykes and gneisses in Russian Karelia of the Fennoscandian Shield—New paleomagnetic, isotope age and geochemical investigations: Precambrian Research, v. 144, p. 239–260, doi: 10.1016/j.precamres.2005.11.005.

Muehlenbachs, K., 1998, The oxygen isotopic composition of the oceans, sediments and the seafloor: Chemical Geology, v. 145, p. 263–273.

Ojakangas, R.W., Marmo, J.S., and Heiskanen, K.I., 2001, Basin evolution of the Paleoproterozoic Karelian Supergroup of the Fennoscandian (Baltic) Shield: Sedimentary Geology, v. 141–142, p. 255–285, doi: 10.1016/S0037-0738(01)000793.

Pesonen, L.J., Elming, S.-A., Mertanen, S., Pisarevsky, S., D'Agrella-Filho, M., Meert, J., Schmidt, P., Abrahamsen, N., and Bylund, G., 2003, Paleomagnetic configuration of supercontinents during the Proterozoic: Tectonophysics, v. 375, p. 289–324, doi: 10.1016/S0040-1951(03)00343-3.

Rumble, D., and Yui, T.F., 1998, The Qinglongshan oxygen and hydrogen isotope anomaly near Donghai in Jiangsu Province, China: Geochimica et Cosmochimica Acta, v. 62, p. 3307–3321, doi: 10.1016/S0016-7037(98)00239-7.

Serebryakov, N.S., Astafiev, B.Y., Voinova, O.A., and Presnyakov, S.L., 2007, Single zircon dating of metasomatites from the Belomorian Belt: Doklady Earth Sciences, v. 413A, p. 388–392.

Terekhov, E.N., 2007, REE distribution in corundum bearing and other metasomatic rocks during exhumation of metamorphic rocks of the Belomorian Belt of the Baltic Shield: Geochemistry International, v. 45, p. 364–380, doi: 10.1134/S0016702907040040.

Valley, J.W., 2001, Stable isotope thermometry at high temperatures: Reviews in Mineralogy and Geochemistry, v. 43, p. 365–413, doi: 10.2138/gsrmg.43.1.365.

Visotskii, S.V., Ignatiev, A.V., Yakovenko, V.V., and Karabtsov, A.A., 2008, Anomalous light oxygen isotope composition in minerals of corundum-bearing rocks in northern Karelia: Doklady Earth Sciences, v. 423, p. 1216–1219, doi: 10.1134/S1028334X08080072.

Watson, E.B., and Cherniak, D.J., 1997, Oxygen diffusion in zircon: Earth and Planetary Science Letters, v. 148, p. 527–544, doi: 10.1016/S0012-821X(97)00057-5.

Zhao, G.C., Cawood, P.A., Wilde, S.A., and Sun, M., 2002, Review of global 2.1–1.8 Ga orogens: Implications for a pre-Rodinia supercontinent: Earth-Science Reviews, v. 59, p. 125–162, doi: 10.1016/S0012-8252(02)00073-9.

Zheng, Y.-F., Wu, Y.-B., Chen, F.K., Gong, B., Li, L., and Zhao, Z.-F., 2004, Zircon U-Pb and oxygen isotope evidence for a large-scale ^{18}O depletion event in igneous rocks during the Neoproterozoic: Geochimica et Cosmochimica Acta, v. 68, p. 4145–4165, doi: 10.1016/j.gca.2004.01.007.

Manuscript received 15 December 2009
Revised manuscript received 16 December 2009
Manuscript accepted 11 February 2010

Printed in USA

DR2010170
Electronic supplementary materials to the Paper by Bindeman, Schmitt and Evans.

Samples

All ruby corundum-bearing samples (K1,2,3,5) come from two trenches that expose a single 300x40 m outcrop (locality 4, Fig.1) in the middle of the Khitostrov island with coordinates 66°N 20' (33''-37'') and 33°E 02' (20-23'') (Fig. A3-A4) while the corundum samples (K4,K6) come from the west of this outcrop near the shore (66°N 20'35'' 33°E02'20'') that embed the above corundum-bearing "matasomatites" bodies.

Analytical technique

Oxygen isotope analyses of plagioclase, rubies, kyanite, biotite, amphibole, garnet, zircon, monazite, and rutile relied on 0.5-2 mg aliquots and were performed at the University of Oregon stable isotope lab using CO_2-laser fluorination (Bindeman, 2008). We concentrated on single grain and core and rim parts of the same grain analyses where size permitted (shown in pink in Table 1). Small mineral grains of zircon, monazite and rutile were run as bulk and size fraction mixtures. Samples were heated up by a NewWave 35Watts laser in the presence of purified BrF_5 reagent to liberate oxygen. The gas generated in the laser chamber was purified through a series of cryogenic traps held at liquid nitrogen temperature, and a mercury diffusion pump to remove traces of fluorine gas. Oxygen was converted to CO_2 gas in a small platinum-graphite converter, the yields were measured, and then CO_2 gas was analyzed on a MAT 253 mass spectrometer in a dual inlet mode. Four to seven Gore Mt garnet standard ($\delta^{18}O$= 5.75‰) were analyzed together with the unknowns during each of seven analytical sessions. Day-to-day $\delta^{18}O$ variability of standards ranged from being 0.1 to 0.35‰ lighter than their reference values and the measurements of unknowns were adjusted to correct for day-to-day variability. The precision on standards is better than 0.1‰ 1 st dev on average.

Because samples were significantly lighter in $\delta^{18}O$ than our standard (and no standard as negative as the reported values exist to our knowledge), one might worry about analytical offsets related to the memory effects. However garnet standard run after –20‰ unknown did not display downward shift by more than –0.1‰ as compared to normal-$\delta^{18}O$ samples run in different data blocks of the same analytical session; we therefore accept that memory effects on the order of 0.1 ‰ could have affected the measured values but we choose not to apply any special corrections other then those outlined above, given the remarkably large $\delta^{18}O$ range found. Mass spectrometry analyses of isotopically negative samples vs a standard gas should not result in unexpected deltas because calculation of deltas is done using raw ratios.

We additionally performed oxygen isotope measurements for 2 samples using O_2 gas as analyte without converting it to CO_2 in order to check for mass-independent ^{17}O anomaly. This anomaly could signify potential extraterrestrial (e.g. cometary) origin of ultradepleted $\delta^{18}O$ Karelian gneisses, or Archean mass-independent effects due to atmospheric photolysis. The O_2 measurements are routinely performed at the University of Oregon Stable Isotope lab to characterize mass independent ^{17}O excesses in terrestrial (Martin and Bindeman 2009) and extraterrestrial materials such as HED meteorites (Ruzicka et al. in prep) and we have good calibration procedures for $\Delta^{17}O$. However two measurements yielded $\Delta^{17}O$ =0 permil thus denying the possibility of extraterrestrial or atmospheric photolytic origin.

Hydrogen isotope measurements relied on 1-2 mg of individual and bulk biotite and amphibole crystals and were performed in a continuous flow mode using UHP He carrier gas and TC/EA furnace with glassy carbon (improved after Sharp et al. 2001). We employed three out of four solid standards in three analytical sessions (NBS30 biotite, δD=-66‰, Water Canyon biotite, δD=-106‰, Butte Montana BUD biotite δD=–161.8‰, and RUH2 muscovite, δD=-98.2‰) spanning the range of 95‰ and overlapping with the ranges of the unknowns. We applied three point calibration using offsets between obtained δD values and the quoted values for mica standards run during each analytical session. Instrumental mass fractionation offset were typically between 20 and 30‰ and the magnitude of offset differed by less than 10‰ in

lighter vs. heavy D/H ends. Base on the repeat values of standards, the 1 st deviation ranged in the ±2-3‰ range. Furthermore, in the beginning of each analytical session we applied H3 factor at different pressure of the carrier gas to correct for different peak heights.Water concentrations were determined by mass H_2 peak integration and the uncertainty is estimated to be ±0.1wt% based on standards. As biotite and amphibole have ~4-4.5 and ~2 wt‰ H_2O respectively, the amount of alteration by chlorite (a phase with ~10wt% H_2O) can be estimated based on water concentration (high-H_2O samples, Table DR1b).

Whole-rock major and trace element concentrations were performed at the Washington State University by XRF and ICPMS methods (Table DR3, Fig. DR2).

Ion microprobe U-Pb dating of zircons and investigation of 18/16 ratio was performed at UCLA by Cameca 1270 large radius ion microprobe using standard procedures outlined in Schmitt et al. (2003) and Bindeman et al. (2006). Zircons were extracted from two crushed samples using standard density separation procedures involving heavy liquids and magnetic Franz separator. Extracted zircons were mounted in the conductive indium metal and polished to expose zircon cores. Dating included O2+ primary beam, initial presputtering and calibrations were performed using AS3 standard (Table DR2a).

Oxygen isotope analyses were performed after repolishing the indium mount down by ~10 microns (to remove pit topography and oxygen implanted during U-Pb dating analysis), used Cs primary beam, 25 micron beam size and targeted approximately the same spots as those used for dating. Relatively large beam size and repolishing likely resulted in core/rim overlap in some analyses. Measurements of two zircon standards (AS3, n=20, and KIM5, n=5) run before, during and after the unknowns, yielded IMF =2.91±0.08‰, and no $\delta^{18}O$ drift.

Monazite U-Th-Pb dating (Table DR2b) was performed on University of Oregon's Cameca SX100 electron microprobe using 300nA current, analytical and age derivation protocol from Montel et al. (1996).

Bindeman, I.N. 2008. Oxygen Isotopes in Mantle and Crustal Magmas as Revealed by Single Crystal Analysis. MINERALS, INCLUSIONS AND VOLCANIC PROCESSES, Reviews in Mineralogy and Geochemistry, Vol. 69, pp. 445-478.

Bindeman I.N., Schmitt A.K., Valley J.W. (2006) U-Pb zircon geochronology of silicic tuffs from the Timber Mt/Oasis Valley caldera complex, Nevada: rapid generation of large-volume magmas by shallow-level remelting. Contrib. Mineral. Petrol. 152:649-665.

Schmitt, A.K., Grove, M., Harrison, T.M., Lovera, O., Hulen, J.B., Walters, M., 2003. The Geysers–Cobb mountain magma system California (Part 1): U–Pb zircon ages of volcanic rocks conditions of zircon crystallization and magma residence times. Geochim. Cosmochim. Acta 67, 3423–3442.

Martin, E; Bindeman, I (2009) Mass-independent isotopic signatures of volcanic sulfate from three supereruption ash deposits in Lake Tecopa, California. Earth Planet Sci Lett. 282: 102-114.

Montel, JM; Foret, S; Veschambre, M, Nicollet C, Provost A.1996. Montel Electron microprobe dating of monazite. Chem. Geol. 131: 37-53.

Sharp, ZD; Atudorei, V; Durakiewicz, T. 2001. A rapid method for determination of hydrogen and oxygen isotope ratios from water and hydrous minerals. Chem. Geol. 178: 197-210.

Table DR1-a Oxygen isotope analyses of individual minerals (red) and bulk mineral separates (blue) in crystal clusters
K-1-3 means sample K1, cluster 3, see Fig. A4

	δ18O, VSMOW, ‰							
	Monazite	Plag	Garnet	Amph	Zircon	Ruby	Biotite	Kyanite	Rutile
Sample K-1 Corundum plagiogneiss									
K-1		-19.25	-23.47	-21.74		-23.76	-22.52		-23.45
K-1		-18.24	-23.44	-21.37		-24.40			
K-1						-24.44			
K-1						-24.12			
K-1						-24.42			
K-1-1		-19.65				-24.30	-18.25		
K-1-2		-20.90				-24.04	-16.85		
K-1-3		-19.24				-24.16	-17.11		
K-1-4		-20.96				-24.21	-18.29		
K-1-5		-20.69				-22.13	rim of big		
Sample K-2 Corundum plagiogneiss									
K-2-1		-21.02	-22.44			-25.79	-21.65		
K-2-2						-26.32			
K-2-3		-23.45				-25.89			
K-2-4		-20.92	-24.65			-26.14	-23.57		
K-2-4				-24.84		-24.84			
Sample K-3 Corundum plagiogneiss						rim big			
K-3-1		-21.47		-25.52		-25.63	-25.04		-26.97
K-3-1						-24.29	core of big		
K-3-1						-23.62	rim of big		
K-3-1						-23.47	core of big		
K-3-2		-19.74				-22.84			
K-3-2						-23.85			
K-3-3		-22.50				-26.07			
K-3-5						-25.79	-16.67		
Sample K-4 Kyanite-Corundum plagiogneiss, melanocratic									
K-4		-15.28				-17.74	-18.06	-19.97	-21.87
K-4-2	-17.45	-14.76				-18.51	-18.09		
K-4-2						-18.09			
K-4-3		-15.76				-18.44	-17.89	-19.83	
K-4-3							-17.53		
K-4-4		-14.75				-18.127	-18.10	-20.01	
								-18.09	
Sample K-5 Corundum plagiogneiss									
K-5		-20.05	-23.23	-22.88	-17.97	-23.06			-27.9
K-5		-19.75	-22.90	-22.56	-19.85	-22.74			
K-5		-20.44			-15.00				
Sample K-6 Kyanite-Corundum plagiogneiss, leucocratic									
K-6		-17.33				-18.57	-19.62	-19.96	-20.35
K-6								-20.00	
								-20.59	

Sample K-3 run as O2 gas

		δ18O, ‰	d17O	Δ17O = 1000*Ln[(δ17O/1000)+1] - 0.5259*1000*Ln[(δ18O/1000)+1]
K-3	Ruby-1	-27.04	-14.36	-0.05 ±0.036
K-3	Plag-1	-20.63	-10.96	-0.06 ±0.037

Table DR1-b
Hydrogen Isotope analyses of biotite, amphibole, and alteration minerals

		wt% H2O	dD
K-1	Amph	2.26	-159.1
K-1	Amph	2.36	-155.1
K-1	Amph	2.4	-143.5
K-1	Amph	1.8	-156.6
K-1	Biotite-1	4.93	-117.5
K-1	Biotite-1	4.62	-128.0
K-1	Biotite-1	4.01	-83.4
K-1	Biotite	4.1	-147.7
K-1	Biotite	4.8	-128.2
K-1	Biotite	3.6	-90.1
K-2	chlorite	10.6	-56.2
K-2	chlorite	11.6	-54.9
K-2-2	Biotite	3.9	-85.1
K-2-2	Biotite	3.8	-93.3
K-2-1	Biotite	4.3	-100.6
K-2-4	Biotite	3.3	-104.5
K-2-4	Amph	2.5	-139.8
K-3	Amph	3.0	-166.3
K-3-1	Amph	3.1	-132.0
K-3	Biotite	5.6	-110.0
K-3	Biotite	6.1	-93.4
K-3	Biotite	5.9	-88.5
K-3	Biotite-1	4.6	-188.9
K-3	Amph-1	2.6	-159.0
K-4	Biotite	3.7	-131.9
K-4	Biotite	3.7	-133.6
K-4-2	Biotite	3.7	-128.6
K-4-2	Biotite	3.7	-128.9
K-4-3	Biotite	3.7	-138.5
K-5	Amph	2.7	-142.2
K-5	Amph	2.8	-133.1
K-5	Amph	2.4	-144.9
K-6	Biotite	3.7	-131.0
K-6	Biotite	3.7	-129.7

Table DR2a: Sample K-5 U-Pb zircon geochronology and Oxygen Isotope analysis by ion microprobe

zircon	spot	comment	d18O	±1 s	206Pb*/ 238U	206Pb*/ 238U	207Pb*/ 235U	207Pb*/ 235U	207Pb*/ 206Pb*	Correlation 207Pb*/ 206Pb*	Age (Ma) of Concordia Ellipses	Age (Ma) 206Pb/ 238U	Age (Ma) 206Pb/ 238U	Age (Ma) 207Pb/ 235U	Age (Ma) 207Pb/ 235U	Age (Ma) 207Pb/ 206Pb	% Radiogen 207Pb/ 206Pb	Th/ 206Pb	Th/ U	1st	U	Th
				1 s.dev.*		1 s.e.		1 s.e.		1 s.e.			1 s.e.		1 s.e.		1 s.e.			1 s.e.	ppm	ppm
1	1	rim	-24.8	0.37	0.3573	0.0119	5.492	0.197	0.1115	0.0010	0.970	1969	57	1899	31	1824	16	99.6	0.027	0.0014	470	12.6
1	2	core	-25.1	0.37	0.3431	0.0096	5.337	0.154	0.1128	0.0010	0.954	1901	46	1875	25	1846	16	99.7	0.013	0.0009	380	4.8
1	3	core	-26.2	0.37	0.3186	0.0113	4.929	0.172	0.1122	0.0010	0.967	1783	55	1807	29	1836	16	99.4	0.026	0.0015	390	10.1
10	1	rim	3.0	0.37	0.4097	0.0096	9.068	0.222	0.1605	0.0010	0.969	2213	44	2345	22	2461	10	99.6	0.034	0.0011	920	31.2
10	2	core	7.3	0.37	0.5197	0.0162	12.86	0.41	0.1794	0.0006	0.995	2698	69	2669	30	2648	5	99.9	0.006	0.0004	1,350	7.4
11	1	core	6.4	0.37	0.5218	0.0202	12.71	0.50	0.1766	0.0007	0.995	2707	86	2658	37	2621	6	99.7	0.006	0.0006	940	5.2
11	2	rim	7.8	0.37	0.4884	0.0130	12.01	0.32	0.1783	0.0008	0.987	2564	57	2605	25	2637	7	99.7	0.005	0.0003	1,050	5.2
12	1	core	-26.1	0.37	0.3837	0.0119	6.751	0.231	0.1276	0.0013	0.956	2093	56	2079	30	2065	18	99.4	0.019	0.0009	460	8.6
12	2	rim	-16.9	0.37	0.3266	0.0100	5.151	0.181	0.1144	0.0017	0.908	1822	49	1845	30	1870	27	98.6	0.047	0.0018	410	19.2
13	1	core	4.9	0.37	0.4803	0.0156	11.25	0.35	0.1698	0.0008	0.990	2529	68	2544	29	2556	8	99.7	0.006	0.0005	900	5.0
14	1	rim	3.3	0.37	0.3249	0.0092	5.004	0.153	0.1117	0.0011	0.945	1814	45	1820	26	1827	18	99.4	0.142	0.0025	530	75.2
15	1	core	5.2	0.37	0.4240	0.0150	8.817	0.297	0.1508	0.0011	0.980	2278	68	2319	31	2355	12	99.6	0.039	0.0017	550	21.2
2	1	core	7.1	0.37	0.5133	0.0162	13.15	0.46	0.1858	0.0014	0.980	2671	69	2690	33	2705	12	99.8	0.016	0.0009	660	10.8
2	2	rim	5.4	0.37	0.4695	0.0160	10.98	0.38	0.1696	0.0006	0.995	2481	70	2521	33	2554	6	99.8	0.015	0.0011	670	10.2
3	1	rim	7.1	0.37	0.4821	0.0136	11.53	0.34	0.1735	0.0007	0.990	2536	59	2567	27	2592	7	99.8	0.005	0.0003	850	4.5
3	2	core	5.8	0.37	0.4880	0.0153	11.62	0.37	0.1726	0.0008	0.988	2562	66	2574	30	2583	8	99.8	0.017	0.0010	480	8.0
3	3	rim	5.8	0.37	0.5131	0.0150	12.91	0.38	0.1825	0.0005	0.996	2670	64	2673	28	2676	4	99.9	0.052	0.0012	1,580	81.8
4	1	rim	1.7	0.37	0.3494	0.0117	5.428	0.181	0.1127	0.0014	0.930	1932	56	1889	29	1843	23	99.0	0.017	0.0013	340	5.9
4	2	rim	-2.9	0.37	0.5305	0.0158	13.50	0.41	0.1846	0.0007	0.993	2744	66	2716	29	2695	6	99.9	0.155	0.0015	1,100	170.0
4	3	core	4.9	0.37	0.4618	0.0143	10.81	0.35	0.1698	0.0006	0.993	2447	63	2507	30	2556	6	99.6	0.019	0.0008	1,040	19.7
5	1	core	5.1	0.37	0.5049	0.0168	11.82	0.40	0.1698	0.0009	0.988	2635	72	2590	32	2556	9	99.7	0.057	0.0033	780	44.7
5	2	rim	7.0	0.37	0.4875	0.0295	11.08	0.71	0.1649	0.0029	0.962	2560	128	2530	60	2506	30	99.0	0.088	0.0033	630	55.6
6	1	rim	6.6	0.37	0.4443	0.0126	10.95	0.32	0.1787	0.0005	0.996	2370	56	2519	27	2641	4	99.6	0.024	0.0009	1,060	25.4
6	2	core	4.6	0.37	0.4478	0.0129	11.03	0.32	0.1787	0.0007	0.991	2385	57	2526	27	2641	6	99.6	0.019	0.0010	900	16.8
6	3	rim	3.7	0.37	0.4420	0.0133	10.86	0.34	0.1782	0.0010	0.986	2360	59	2511	29	2636	9	99.8	0.009	0.0004	1,110	10.4
7	1	rim	-24.1	0.37	0.3458	0.0097	5.335	0.166	0.1119	0.0010	0.964	1914	47	1875	27	1831	15	99.6	0.011	0.0009	450	5.1
7	2	core	-23.9	0.37	0.3486	0.0121	5.327	0.186	0.1108	0.0007	0.981	1928	58	1873	30	1813	12	99.5	0.008	0.0006	460	3.5
7	3	rim	-24.4	0.37	0.3201	0.0098	4.972	0.162	0.1127	0.0012	0.944	1790	48	1815	28	1843	19	99.5	0.017	0.0011	460	7.8
8	1	core	6.1	0.37	0.4560	0.0131	10.69	0.32	0.1700	0.0011	0.978	2422	58	2496	28	2557	11	99.8	0.006	0.0005	630	3.6
8	2	rim	6.5	0.37	0.4726	0.0158	10.75	0.37	0.1650	0.0013	0.971	2495	69	2502	32	2507	14	99.7	0.007	0.0008	510	3.4
9	1	rim	4.7	0.37	0.4665	0.0141	11.31	0.36	0.1758	0.0006	0.994	2468	62	2549	30	2613	6	99.7	0.088	0.0026	730	64.4
9	2	rim	5.7	0.37	0.5131	0.0135	12.67	0.34	0.1791	0.0015	0.952	2670	58	2656	26	2645	14	99.8	0.077	0.0015	1,010	77.5
9	3	core	6.3	0.37	0.4976	0.0138	12.31	0.35	0.1794	0.0007	0.991	2603	60	2628	26	2648	6	99.8	0.071	0.0015	970	69.0

* 1 st dev is based on measurements of two zircon standards (AS3, n=20, and KIM5, n=5) run before, during and after the unknowns, IMF =2.91±0.08‰ , no d18O drift was observed

Zircon 4

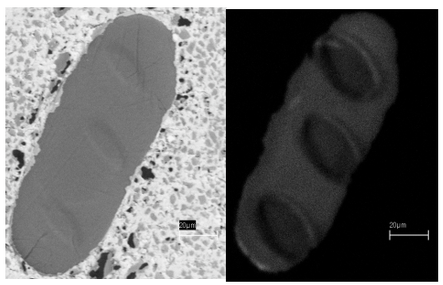

Zircon 14

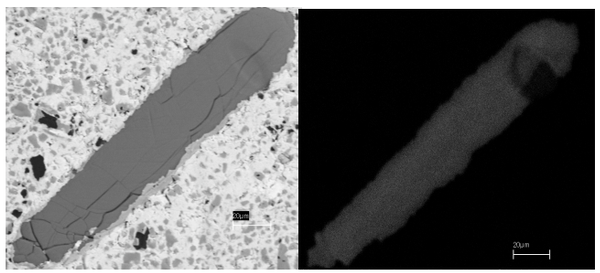

Zircon 12

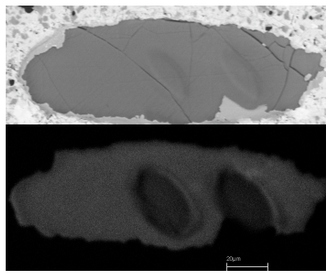

BSE and CL images of selected zircons pressed in indium mount

Table DR2b Sample K-4 Monazite geochronology determined by the electron microprobe

	Pb			Th			U			Montel		
Line nun	Conc (pp	% fit err.	LOD (ppm	Conc (ppm)	% fit err.	LOD (ppm)	Conc (ppm)	% fit err.	LOD (ppm)	Age	+	-
245	4718	2.24842	181.7	36435.0	0.631682	243.8	4360.3	1.59602	125.85	1923.6	54.3	54.3
246	4019	2.60654	185.3	31703.6	0.688575	242.1	4211.6	1.64099	125.45	1831.9	60.2	59.3
247	4116	2.54969	184.8	30954.8	0.70157	245.1	4019.4	1.71319	125.87	1925.4	62.6	61.6
248	4428	2.37979	182.8	33952.7	0.659599	242.7	4216.1	1.62727	124.19	1916.9	58.4	57.5
249	4018	2.58612	183.2	31943.7	0.687226	244.6	4083.7	1.68918	125.83	1840.7	58.5	58.5
250	4350	2.42429	183.8	34303.9	0.654733	241.9	4146.3	1.66248	125.38	1883.3	58.3	57.4
251	3799	2.71624	183.6	28281.7	0.744137	245.4	4218.8	1.63701	125.29	1862.7	64.0	62.9
252	4469	2.36409	183.2	36359.2	0.6327	244.2	4416.8	1.55955	123.8	1828.2	54.8	54.0
253	4643	2.27988	181.9	35808.7	0.638687	244.0	4327.9	1.60457	125.69	1921.5	56.4	55.5
254	4971	2.16477	183.2	39849.4	0.598195	245.4	4267.7	1.62758	126.08	1917.0	53.6	52.9
255	4523	2.34366	183.5	37185.8	0.625466	246.8	4505.4	1.54782	125.47	1812.0	53.6	51.6
256	4417	2.37841	182.1	32975.4	0.671874	242.7	3964.9	1.71909	124.49	1980.4	60.7	57.5
257	4879	2.21784	185.8	38663.8	0.609442	245.2	4180.6	1.65317	125.7	1932.4	55.3	54.5
258	5018	2.14001	182.1	38729.3	0.606696	241.8	4180.1	1.64883	125.24	1980.1	52.5	54.3
259	4657	2.31163	186.5	39330.0	0.602017	243.6	4134.5	1.66966	125.76	1836.7	54.0	53.3
260	4660	2.28	182.8	37738.7	0.618291	244.5	3983.6	1.7249	125.79	1905.8	55.9	55.1
261	4534	2.32332	181.7	36092.2	0.637056	246.4	3832.4	1.77703	125.11	1934.3	55.8	57.4
262	5124	2.10655	182.6	38309.7	0.610926	241.9	4849.3	1.45363	125.53	1950.9	53.0	52.4
263	5639	1.95121	183.0	44063.9	0.561897	244.6	5319.8	1.36321	128.19	1899.9	47.8	47.2
264	5644	1.94764	182.6	45389.0	0.552742	246.7	5387.9	1.33274	126.02	1859.3	46.4	45.8
265	6052	1.83481	181.6	47841.1	0.534181	244.0	5327.1	1.34879	126.47	1922.7	43.4	45.2
266	5937	1.86281	181.5	46120.3	0.545963	243.6	5584.0	1.29177	125.81	1909.0	43.5	45.3
267	5670	1.93605	182.0	44979.8	0.554281	243.5	5491.9	1.31378	126.36	1867.7	46.3	45.7
268	6704	1.70012	183.2	51281.2	0.512877	245.6	6665.4	1.12524	127.56	1895.7	41.4	40.9
269	4717	2.2535	182.4	39317.5	0.603635	246.2	3941.9	1.74894	126.61	1881.7	54.8	54.0
270	3934	2.63611	183.6	29683.9	0.718102	242.2	4305.5	1.60926	125.47	1856.0	61.5	60.6
271	4030	2.58119	183.5	33589.8	0.665132	244.4	3186.8	2.08744	124.82	1906.3	63.4	62.3
272	4148	2.52484	184.0	35158.5	0.648007	246.7	2926.4	2.24844	124.5	1934.8	61.4	62.6
273	3641	2.83705	185.5	34746.6	0.650638	243.5	3037.6	2.15959	123.43	1716.4	57.1	60.2
274	4003	2.6019	184.0	36667.2	0.631369	247.1	2784.0	2.34129	123.83	1836.1	61.5	60.5
275	3526	2.91373	185.2	34047.0	0.659601	244.0	2816.0	2.30987	123.32	1718.7	62.9	61.8
276	4471	2.3468	181.3	34858.2	0.648444	242.5	3834.2	1.77012	124.57	1948.6	61.5	53.8
277	4489	2.34692	182.3	36460.5	0.630563	243.0	3981.0	1.72068	125.35	1884.9	56.9	56.0
278	4774	2.23415	182.8	37802.5	0.61782	245.1	4498.0	1.55821	126.5	1884.4	53.9	53.2
279	5901	1.89779	185.7	45596.0	0.550043	244.5	5957.7	1.23499	127.63	1875.5	45.3	44.9
280	4656	2.26288	180.5	33885.9	0.66036	243.0	4495.1	1.54628	125.05	1970.0	57.3	56.5
281	4500	2.35268	183.5	36349.7	0.632942	244.8	4083.8	1.67881	124.94	1879.7	56.6	55.7
282	4662	2.27177	181.9	35945.7	0.638055	245.7	4199.0	1.64134	125.21	1941.1	54.4	56.2
283	4133	2.51432	182.1	32191.8	0.681881	242.4	4182.7	1.63729	124.2	1865.3	59.5	58.6
284	4512	2.34526	183.3	35313.3	0.643475	243.2	4216.2	1.63999	125.69	1902.9	57.2	56.3
285	4459	2.38403	185.0	35031.0	0.648287	245.3	4274.6	1.62048	125.67	1884.2	57.2	56.3
286	4699	2.27219	183.8	34635.4	0.65123	242.9	4332.9	1.5951	124.98	1982.7	55.2	57.3
287	4476	2.3697	184.3	33860.6	0.661308	244.1	4420.4	1.56823	125.03	1912.5	57.8	57.0
288	4126	2.52795	183.2	30374.2	0.707313	242.0	4204.4	1.63511	124.75	1925.3	61.9	60.9
289	4284	2.45675	184.1	3003.2	0.715861	246.2	4430.6	1.55621	124.05	1799.5	23.0	22.8

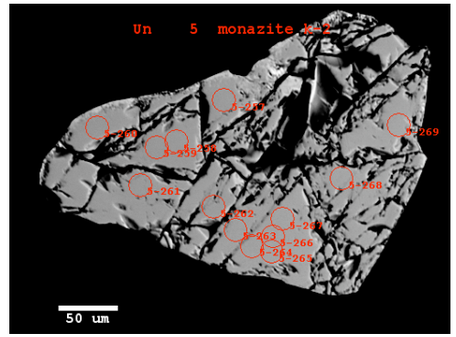

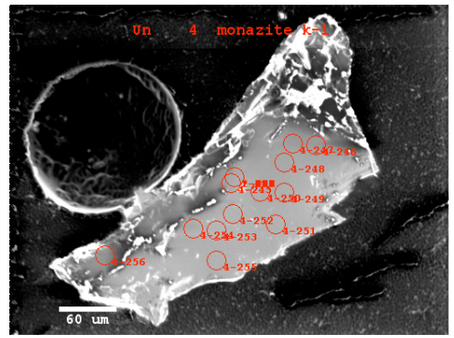

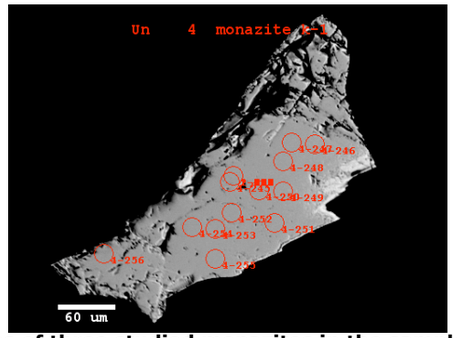

BSE Images of three studied monazites in the sample K-4

Table DR3 XRF and ICP MS analyses of studied rocks

XRF analyses

	K-1	K-2	K-4	K-6
Unnormalized Major Elements (Weight %):				
SiO2	53,09	55,13	44,75	59,99
TiO2	1,019	0,740	1,451	0,268
Al2O3	23,84	23,10	21,87	23,91
FeO*	5,01	4,34	11,98	1,56
MnO	0,040	0,020	0,096	0,008
MgO	3,67	3,82	7,97	1,24
CaO	4,49	4,32	1,60	3,94
Na2O	6,37	6,79	3,04	7,99
K2O	0,43	0,66	5,20	0,87
P2O5	0,041	0,028	0,020	0,112
Sum	98,01	98,95	97,99	99,88
Normalized Major Elements (Weight %):				
SiO2	54,17	55,71	45,67	60,06
TiO2	1,040	0,748	1,481	0,268
Al2O3	24,33	23,34	22,32	23,94
FeO*	5,11	4,39	12,23	1,56
MnO	0,041	0,021	0,098	0,008
MgO	3,75	3,86	8,14	1,24
CaO	4,58	4,37	1,63	3,95
Na2O	6,50	6,87	3,10	8,00
K2O	0,44	0,67	5,31	0,87
P2O5	0,042	0,028	0,021	0,112
Total	100,00	100,00	100,00	100,00
Norm. Corundum	4,94	3,44	8,55	2,93
Ni	167	188	341	56
Cr	324	281	472	131
Sc	17	18	47	4
V	167	136	285	60
Ba	94	207	1962	348
Rb	9	19	250	38
Sr	482	501	186	495
Zr	218	161	222	84
Y	18	12	24	3
Nb	10,9	6,9	6,5	2,9
Ga	34	30	45	30
Cu	4	0	4	1
Zn	37	20	162	24
Pb	13	15	10	16
La	47	45	18	15
Ce	115	103	42	29
Th	17	15	4	3
Nd	49	33	20	12
U	0	2	0	2
Cs	1	5	9	2

ICP-MS analyses

	K-1	K-2	K-4	K-6
Cs	0,39	0,71	7,58	1,17
Rb	8,3	18,0	239,1	36,4
Ba	90	198	1887	339
Th	17,45	15,78	4,60	3,01
U	1,64	1,21	0,98	0,68
Nb	10,45	6,34	5,99	2,26
Ta	0,68	0,38	0,45	0,15
K	3560	5514	43163	7187
La	55,40	50,03	16,34	12,66
Ce	116,14	98,84	34,57	26,29
Pb	10,52	14,35	8,45	14,64
Pr	13,81	10,86	4,12	3,20
Sr	476	493	183	480
Nd	50,44	36,31	15,98	12,71
Sm	9,48	4,95	3,30	2,89
Zr	216	159	220	83
Hf	5,98	4,33	6,11	2,32
Eu	1,56	1,27	0,79	1,52
Ti	6238	4487	8885	1607
Gd	6,43	2,89	3,34	2,10
Tb	0,76	0,37	0,62	0,18
Dy	4,00	2,16	4,22	0,63
Li				
Y	16,64	11,01	23,54	2,33
Ho	0,67	0,45	0,92	0,09
Er	1,58	1,19	2,61	0,21
Tm	0,22	0,17	0,40	0,03
Yb	1,33	1,06	2,47	0,17
Lu	0,21	0,17	0,42	0,03
Sc	19,6	18,6	48,9	4,4

Fig. DR1. Hydrogen and oxygen isotope analyses of biotite and amphibole crystals extracted from crystal clusters (see Tables DR1a and b for analyses). The range of δD and $\delta^{18}O$ values is interpreted here to indicate retrogressive exchange of initially ultra-low (ca –24 to –30‰ $\delta^{18}O$, -170 to -250‰ δD) protoliths with a variety of higher $\delta^{18}O$ and δD waters.

Amphiboles collectively have lower δD values (down to –167‰, Table DR1b) than biotites, maintain equilibrium $\Delta^{18}O$ fractionations (Fig. 1) and appear less retrogressed and retained greater proportion of the initial Paleoproterozoic ultra-depleted hydrogen. The lowest $\delta^{18}O$ and δD hydrous minerals would support a –28 to –30‰ $\delta^{18}O$ protolith. Yellow field and black dashed line represent inferred primary isotopic ranges of hydrous minerals in the protolith based on $\delta^{18}O$ range in refractory rubies parallel to the meteoric water line in different crystal clusters. The δD values in the primary protolithic micas and amphiboles were offset by -30‰ δD for water-mineral fractionation at metamorphic temperature of 600±100°C that correspond to metamorphic grade; at lower, ca 400°C temperature, the offset will be –50‰. Biotites that are most altered display higher water% (Table A1b) due to the presence of higher δD, higher H_2O chlorite; However, the lowest -189‰ Biotite in sample K-3 appears unaltered.

A retrogressive exchange at high temperatures (more than 300-400°C) is required to explain the isotopic trends and ranges. At low temperatures, hydration and alteration would yield perpendicular trend due to large positive $\Delta^{18}O$(mineral-water). Processes of metamorphic water loss and Rayleigh distillation via devolatilization would also produce more shallow negative slope on this diagram, contrary to the trend observed. Isotopic trends are curved concave up because water contain greater molar proportion of hydrogen than rocks. If modern-day meteoric water is taken as altering fluid, hydrous minerals record 4 to 20% retrogressive exchange, see 1-2% tickmarks on each mixing curve; if seawater ($\delta^{18}O$, δD = 0‰) is taken as altering fluid, then 1 to 5% fluid would suffice. Interaction with primary magmatic water ($\delta^{18}O$ and δD= -60±20‰, $\delta^{18}O$ = -5 to –8‰, e.g. Taylor and Sheppard, 1986) would require 2 to 8% of exchange. Deep magmatic, "metasomatizing" waters have been proposed to widely influence rocks from the Belomorian belt causing formation of metasomatites and pegmatites similar to those in Khitostrov (Terekhov, 2007; Ulyanov et al. 2008, Visotskii et al. 2008).

This diagram, while complex and based on several educated assumptions about the protolith, temperatures, and waters, demonstrates that ultra-low-$\delta^{18}O$, δD Paleoproterozoic protolith was affected by heavier $\delta^{18}O$ waters. Any secondary high-T exchange with any types of subsequent external waters will result in elevated δD values in biotites and amphiboles and also yield slightly higher than equilibrium $\delta^{18}O$ values of micas, noticeable in some crystal clusters on Fig. 1. However, either of these secondary fluids, or their time-integrated combination cannot explain large range of whole-rock $\delta^{18}O$ values, which reflect the primary value of heterogeneous, hydrothermally-altered protolith.

Isotopic fractionations used:

Graham, C.M.; Harmon, R.S.; and Sheppard, S.M.F. (1984) Experimental hydrogen isotope studies: Hydrogen isotope exchange between amphibole and water; Amer. Mineral. 69, 128-138.

Savin, S.M.; and Epstein, S. (1970) The oxygen and hydrogen isotope geochemistry of clay minerals; Geochim. Cosmochim. Acta 34, 43-63

Suzuoki, T.; and Epstein, S. (1976) Hydrogen isotope fractionation between OH-bearing minerals and water; Geochim. Cosmochim Acta 40, 1229-1240.

Zheng, Y.F. (1993) Calculation of oxygen isotope fractionation in hydroxyl-bearing silicates; Earth. Plan. Sci. Lett. 120, 247-263.

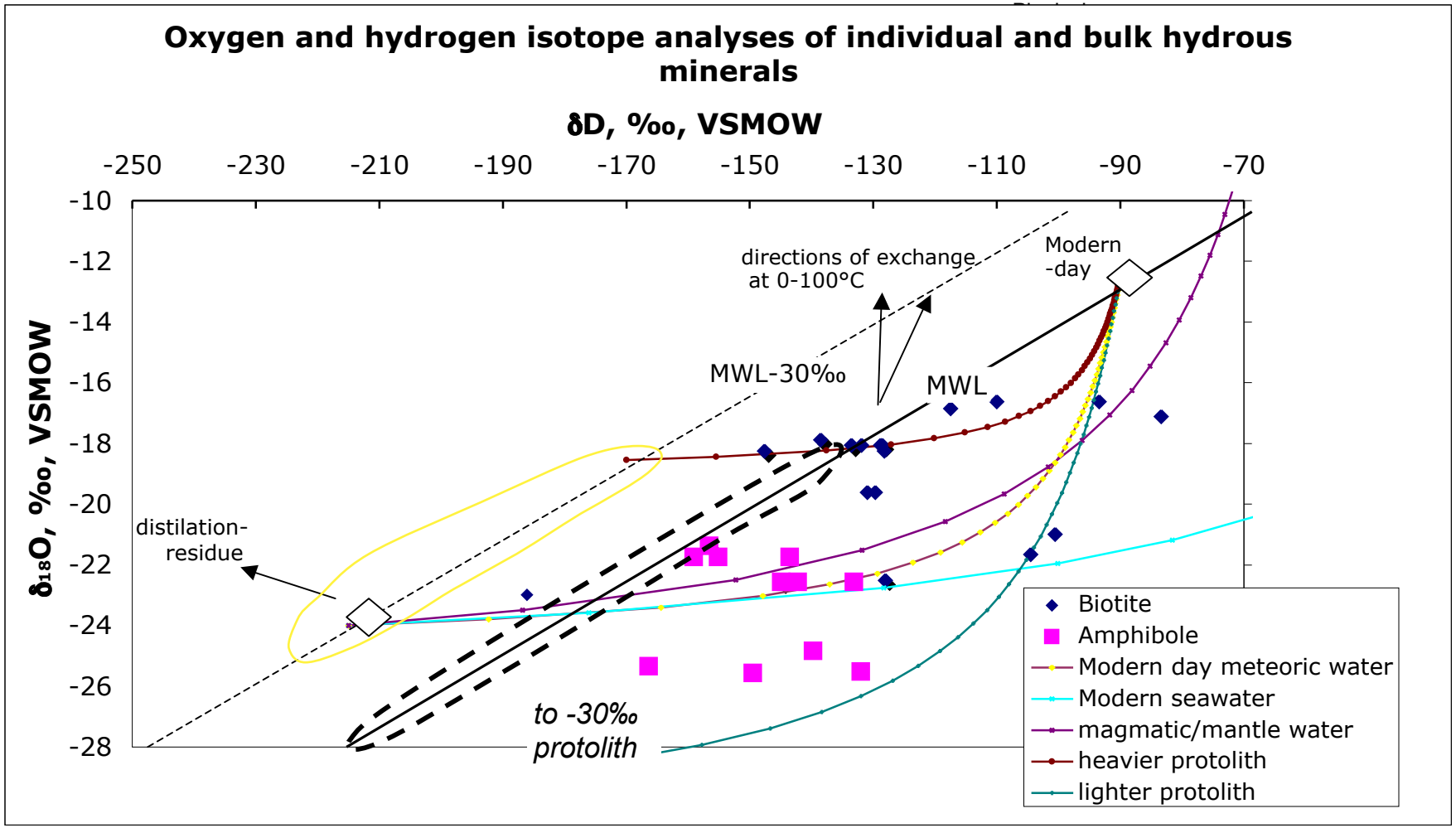

Appendix, Fig. DR1

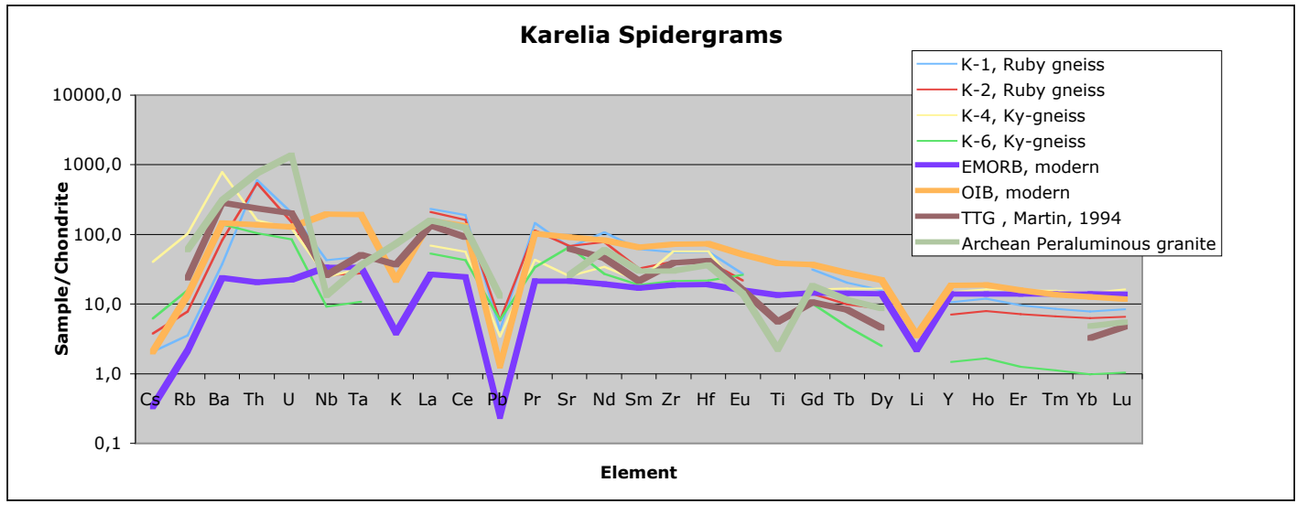

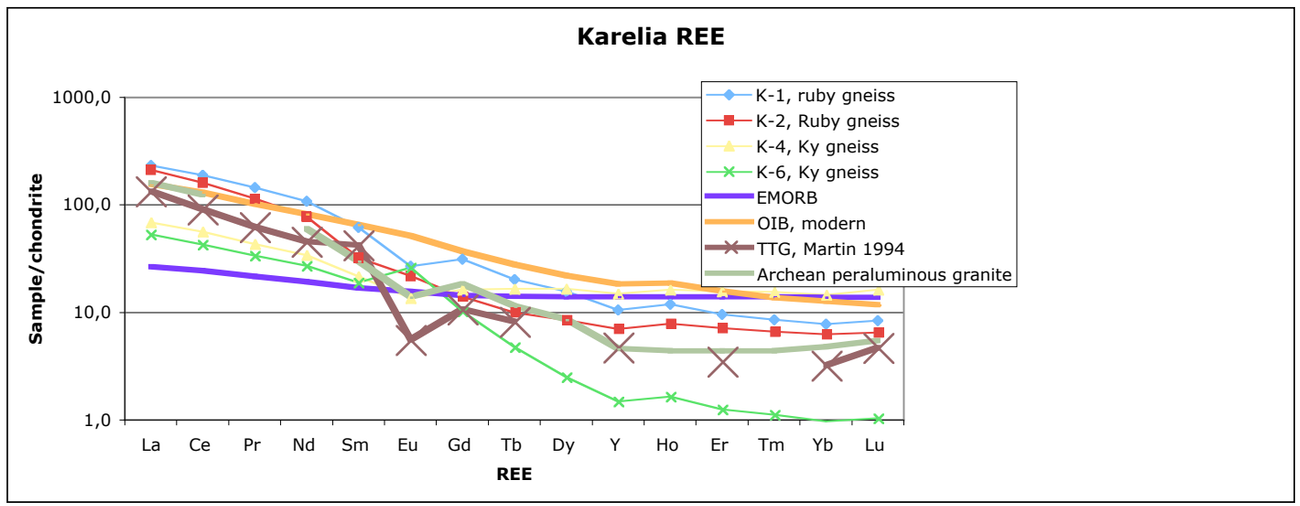

Fig. DR2 Major and trace element analyses of investigated corundum and kyanite plagiogneisses. Figure demonstrates normalized trace elemental pattern as compared to Archean rocks and modern MORB and OIB basalts showing their intermediate to metabasaltic (metagreywacke) composition. The fractionated REE pattern is most consistent with other Archean rock types and derivation within a rift. TTG suites and Archean peraluminous granites are from H. Martin, 1994, The Archean grey gneisses and the genesis of continental crust. in Condie KC Ed Archean crustal evolution, Developments in Precambrian Geology11, Elsevier, pp. 205-260.

Fig. DR3 Field and outcrop photographs
a) Khitostrov outcrop; b) trench across ruby and kyanite-bearing gneisses, c) ruby-bearing plagiogneiss

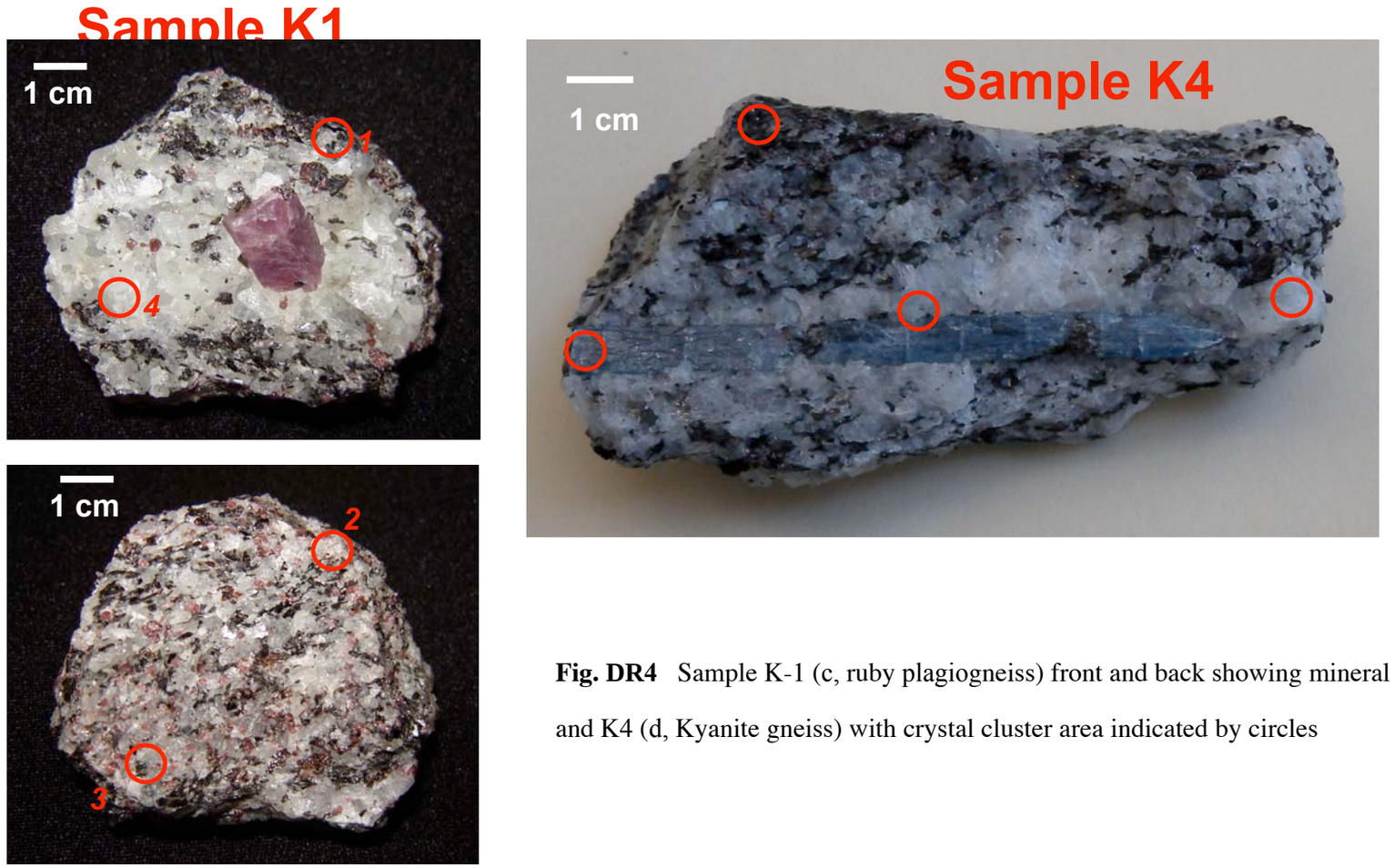

Fig. DR4 Sample K-1 (c, ruby plagiogneiss) front and back showing mineral cluster areas and K4 (d, Kyanite gneiss) with crystal cluster area indicated by circles